JOURNAL OF COMPUTATIONAL PHYSICS **144,** 17–51 (1998)
ARTICLE NO. CP985981

A Local Support-Operators Diffusion Discretization Scheme for Quadrilateral *r-z* Meshes

J. E. Morel, Randy M. Roberts, and Mikhail J. Shashkov

University of California and Los Alamos National Laboratory, Los Alamos, New Mexico 87545

Received February 14, 1997; revised January 13, 1998

We derive a cell-centered 2-D diffusion differencing scheme for arbitrary quadrilateral meshes in *r-z* geometry using a local support-operators method. Our method is said to be local because it yields a sparse matrix representation for the diffusion equation, whereas the traditional support-operators method yields a dense matrix representation. The diffusion discretization scheme that we have developed offers several advantages relative to existing schemes. Most importantly, it offers second-order accuracy even on meshes that are not smooth, rigorously treats material discontinuities, and has a symmetric positive-definite coefficient matrix. The only disadvantage of the method is that it has both cell-center and face-center scalar unknowns as opposed to just cell-center scalar unknowns. Computational examples are given which demonstrate the accuracy and cost of the new scheme relative to existing schemes.

1. INTRODUCTION

The diffusion equation that we seek to solve can be expressed in the general form

$$\frac{\partial \phi}{\partial t} - \vec{\nabla} \cdot D\vec{\nabla}\phi = Q, \tag{1}$$

where t denotes the time variable, ϕ denotes a scalar function that we refer to as the intensity, D denotes a scalar diffusion coefficient, and Q denotes a source or driving function. The boundary conditions for Eq. (1) can be of the Dirichlet, Neumann, or Robin (mixed) type. It is sometimes useful to express Eq. (1) in terms of a vector function, $\vec{F}$, that we refer to as the flux,

$$\vec{F} = -D\vec{\nabla}\phi. \tag{2}$$

We have taken the terms "intensity" and "flux" from the radiative transfer literature [1],

0021-9991/98 $25.00

but we have not explicitly considered the radiative diffusion equation because the subject of this paper relates to essentially any type of diffusion problem.

We define a cell-centered diffusion discretization scheme as one that numerically expresses the integral of Eq. (1) over each spatial cell. In particular, substituting from Eq. (2) into Eq. (1) and integrating that equation over a cell volume, we obtain

$$\int_V \frac{\partial \phi}{\partial t}\, dV + \oint_{\partial V} \vec{F} \cdot \vec{n}\, dA = \int_V Q\, dV, \tag{3}$$

where V denotes the cell volume, ∂V denotes the cell surface, and $\vec{n}$ denotes the outward-directed unit surface normal. Note that we used the divergence theorem to convert the second integral in Eq. (3) from a volume integral to a surface integral. In physical terms, Eq. (3) generally represents a statement of particle or energy conservation over the cell. Thus we can simply state that cell-centered schemes are conservative over each mesh cell.

If one considers only non-orthogonal meshes with material discontinuities, existing vertex-centered diffusion discretizations are generally more advanced than cell-centered discretizations. This is primarily so because of the enormous success of Galerkin finite-element methods [2] and variants of those methods. Nonetheless, there are applications for which cell-centered schemes appear to yield superior accuracy relative to vertex-centered schemes. For instance, when coupling diffusion calculations with cell-centered hydrodynamics calculations, a cell-centered diffusion scheme is highly desirable because it avoids the excessive numerical dissipation which can occur with vertex-centered diffusion schemes [3]. Our new scheme was developed with coupled radiation-diffusion/hydrodynamics applications in mind.

The following could be said of an ideal cell-centered diffusion scheme for 2-D quadrilateral meshes:

(1) It gives second-order accuracy on both smooth and non-smooth meshes either with or without material discontinuities.

(2) It has only cell-center intensity unknowns.

(3) It has a local stencil.

(4) It has a symmetric positive-definite matrix representation for the diffusion equation, i.e., a positive-definite "diffusion matrix."

A local stencil is loosely defined to have coupling only between points that are spatially "close" in some sense. Cell-centered schemes such as those of Kershaw [4] and Pert [5], satisfy properties (2) through (4), but do not satisfy item (1). The scheme of Morel, Dendy, Hall, and White [6] satisfies properties (1) and (3), but does not satisfy properties (2) and (4). In particular, it has face-center intensity unknowns in addition to cell-center intensity unknowns, and it has an asymmetric diffusion matrix. The scheme of Van Beek, Van Nooyen, and Wesseling [7] satisfies properties (2) and (3), but not (1) and (4). In particular, it is non-convergent whenever the transverse component of the flux is discontinuous across a material interface. In addition, its diffusion matrix is asymmetric. Aavatsmark, Barkve, Bøe, and Mannseth [8] have introduced two diffusion discretizations that they refer to as the U-method and the O-method. The U-method satisfies properties (2) and (3), but it has an asymmetric diffusion matrix. The O-method also satisfies properties (2) and (3), and it appears to yield a symmetric diffusion matrix in practice. However, it has not been proven that it will always yield a symmetric diffusion matrix. Neither the U-method nor the O-method was actually

shown to converge with material discontinuities. The support-operators scheme of Shashkov and Steinberg [9] (derived only in x-y geometry) satisfies properties (1), (2), and (4), but does not satisfy property (3). Their scheme has a dense diffusion matrix, which arises from a dense gradient matrix multiplied by a local divergence matrix. This difficulty can be circumvented for time-dependent calculations by transforming the dense equations into a local form in which the unknowns are the normal components of the flux located at face centers. For steady-state calculations, Shashkov and Steinberg recommend that the dense intensity-based system be solved using a conjugate-gradient approach. This would initially appear to require the multiplication of a vector and a dense matrix during each conjugate-gradient iteration. However, Shashkov and Steinberg show that this dense matrix-vector multiply can be effectively performed by solving a sparse diagonally dominant SPD matrix system. This suggests a nested conjugate-gradient solution process: an outer conjugate gradient process solves the dense intensity-based system, and an inner conjugate-gradient process solves the sparse system associated with the dense matrix-vector multiply required for each outer conjugate-gradient iteration. Although this approach would probably be much more efficient than actually performing a dense matrix-vector multiply, it could nonetheless be quite expensive relative to simply solving a sparse SPD matrix representation for the diffusion equation.

The purpose of this paper is to use the support-operators approach [9] to derive a cell-centered diffusion discretization scheme for arbitrary quadrilateral meshes in r-z geometry. As previously indicated, the traditional cell-centered support-operators methodology used by Shashkov and Steinberg [9] leads to a dense diffusion matrix on non-orthogonal grids. Here we introduce a new variant of the cell-centered support-operators methodology which always leads to a local diffusion stencil at the expense of additional face-center intensity unknowns. Hence we refer to this new variant as a "local" support-operators method. We stress that the local cell-center/face-center system that we obtain is equivalent to the dense cell-center system obtained with the traditional support-operators methodology in the sense that both systems yield the same cell-center intensity solution. Thus our new diffusion scheme represents a generalization to r-z geometry of the X-Y geometry scheme of Shashkov and Steinberg [9]. Interestingly, our new scheme is very similar to the scheme of Morel, Dendy, Hall, and White (MDHW) [6]. In particular the two schemes have the same unknowns, the same cell-center stencil, and nearly the same face-center stencil (7-point for the MDHW scheme, versus 9-point for the new scheme.) Of course, the significant difference between the schemes is that our new scheme has a symmetric positive-definite diffusion matrix whereas the MDHW scheme has an asymmetric diffusion matrix. The similarity between these schemes suggests that the MDHW multigrid solution technique [6] could be used to construct a multigrid preconditioner for our scheme. Indeed, we have developed such a preconditioner and it is later shown that it performs quite well.

In summary, our new diffusion discretization scheme has the following properties:

- It gives second-order accuracy on both smooth and non-smooth meshes either with or without material discontinuities.
- It has both cell-center and face-center intensity unknowns.
- It has a local stencil.
- It has a symmetric positive-definite matrix representation for the diffusion operator.

Note that it satisfies ideal properties (1), (3), and (4), but not (2). We know of no finite-difference cell-centered scheme that satisfies all four ideal properties. We believe that our

new scheme has the best combination of ideal properties of any previous finite-difference scheme.

Although basis functions do not appear in our formalism, the support-operators method might be related to mixed finite-element methods [10]. For instance, mixed finite-element schemes preserve the integral of Eq. (1) over each spatial cell and have primary intensity unknowns at the cell centers. Unfortunately, the matrix associated with the pure cell-center system is generally indefinite and thus difficult to solve. As long as continuity of the intensity and the normal flux component need only exist at the center of each cell face rather than at vertices, this difficulty can be circumvented by eliminating continuity as a trial-space requirement and imposing it via Lagrange multipliers. These multipliers can be shown to be equivalent to face-center intensity unknowns. This results in an SPD system of equations for both the cell-center and cell-edge intensity unknowns. The similarity of this formulation to our local support-operators formulation in terms of cell-wise integration and the location of the intensity unknowns is striking and suggests the possibility of a deeper connection. This question should be investigated in the future. Arbogast *et al.* [11] and Cai *et al.* [12] have very recently developed mixed finite-element methods that appear to be somewhat similar to our support-operators method.

The remainder of this paper is organized as follows. We next explain the central theme of the support-operators method, describe our local methodology, and apply it to the simple case of a rectangular mesh in r-z geometry. This is followed by a derivation of our method for general quadrilateral meshes in r-z geometry. Our multigrid-preconditioned solution technique for logically rectangular meshes is then described. Finally, computational results are given, followed by conclusions and recommendations for future work.

2. THE SUPPORT-OPERATORS METHOD

In this section we describe the support-operators method. It is convenient at this point to define a modified gradient operator given by $-D\vec{\nabla}$. The diffusion operator of interest is given by the product of the divergence operator and the modified gradient operator: $-\vec{\nabla} \cdot D\vec{\nabla}$. The support-operators method is based upon the following three facts:

- Given appropriately defined scalar and vector inner products, the divergence and modified gradient operators are adjoint to one another.
- The adjoint of an operator varies with the definition of its associated inner products, but is unique for fixed inner products.
- The product of an operator and its adjoint is a self-adjoint positive-definite operator.

The mathematical details relating to these facts are given in [9]. Our support-operators method can be described in the simplest terms as follows:

(1) Define discrete scalar and vector inner products that approximate the analytic inner products on a single arbitrary cell.

(2) Define the discrete version of the divergence operator on a single arbitrary cell.

(3) Use the adjoint property to define the discrete version of the modified gradient operator on a single arbitrary cell.

(4) Obtain the global matrices by connecting adjacent mesh cells in such a way as to ensure that the adjoint relationship is maintained over the whole grid. This simply amounts to enforcing continuity of intensity and flux at the cell interfaces.

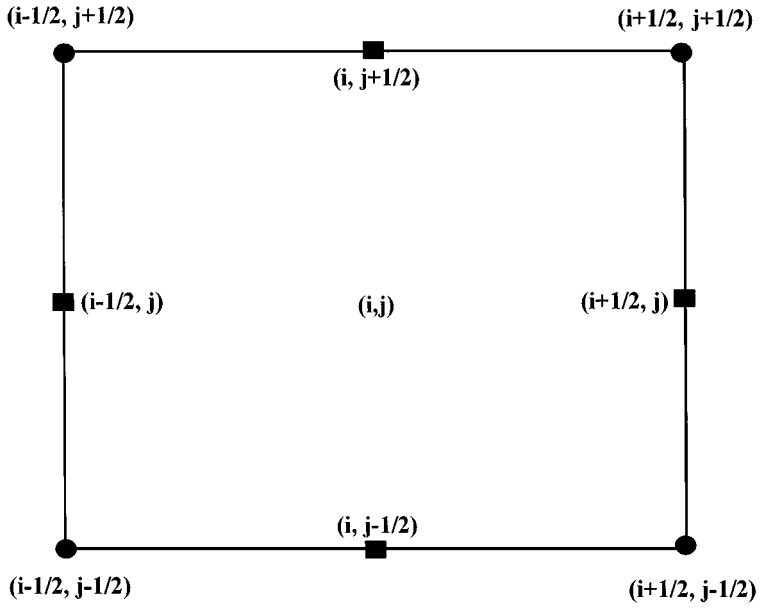

FIG. 1. Global coordinate and mesh indexing. The global indexing for mesh cell i, j is illustrated. Vertices are marked by circles and carry half-integer indices. Face centers are marked by squares and carry both integer and half-integer indices. Cell centers are marked by a triangle and carry integer indices. The fundamental mesh coordinates lie at the vertices. If the mesh is orthogonal, the r-coordinates need carry only the index i and the z-coordinates need carry only the index j, but if the mesh is non-orthogonal, both indices are required for each coordinate pair.

(5) Combine the divergence matrix and the modified gradient matrix to obtain the diffusion matrix.

To make this process concrete, we generate the diffusion matrix for a rectangular mesh in r-z geometry. Our first step is to define the discrete unknowns. The global coordinate and mesh indexing is illustrated in Fig. 1. The local mesh indexing (local to each cell) is shown in Fig. 2. Each mesh cell is assumed to be homogeneous, but material properties may vary between cells. As shown in Fig. 3, the intensities (scalars) are defined to exist at both cell center, $(\phi^C_{i,j})$, and face-center, $(\phi^R_{i,j}, \phi^B_{i,j}, \phi^L_{i,j}, \phi^T_{i,j})$. Note that the use of local indices implies that a quantity is uniquely associated with a single cell. Thus, for instance, one should not necessarily assume that $\phi^R_{i,j} = \phi^L_{i+1,j}$. As shown in Fig. 4, the vectors are defined in terms of surface-normal components located at the midpoints of the cell faces, $(f^R_{i,j}, f^B_{i,j}, f^L_{i,j}, f^T_{i,j},)$. For instance, $f^R_{i,j}$ denotes the dot product of $\vec{F}$ with the outward-directed unit surface normal located at the center of the right face of cell i, j. The other surface-normal vector components are defined analogously. Since it takes two components to define a full vector, the full vectors are considered to be located at the cell corners, $(\vec{F}^{RB}_{i,j}, \vec{F}^{BL}_{i,j}, \vec{F}^{LT}_{i,j}, \vec{F}^{TR}_{i,j})$. As shown in Fig. 5, each corner vector has surface-components located on the two faces that share that corner, e.g.,

$$\vec{F}^{RB}_{i,j} = \left(f^R_{i,j}, f^B_{i,j}\right). \tag{4}$$

The other corner vectors are defined analogously.

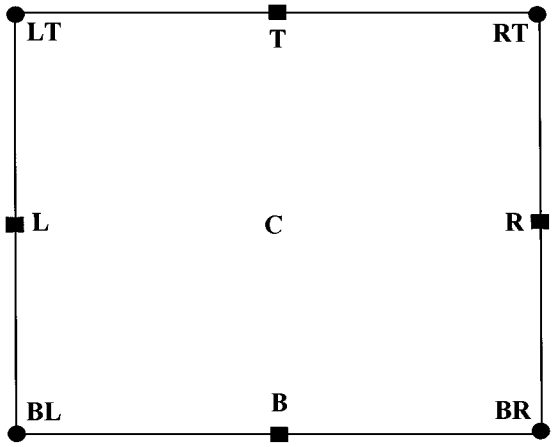

FIG. 2. Local mesh indexing. Corners are denoted by TR (top-right), RB (right-bottom), BL (bottom-left), and LT (left-top). Faces are denoted by R (right), B (bottom), L (left), and T (top). Note that local indexing can accommodate multiple unknowns at the same location. For instance, the intensity on the right face of cell i, j need not necessarily be equal to the intensity on the left face of cell $i+1, j$.

As explained in [9], the adjoint relationship between the modified gradient and divergence operators is embodied in the integral identity

$$\oint_{\partial V} \phi \vec{H} \cdot \vec{n}\, dA - \int_V D^{-1} \vec{H} \cdot D\vec{\nabla}\phi\, dV = \int_V \phi \vec{\nabla} \cdot \vec{H}\, dV, \tag{5}$$

where ϕ is an arbitrary scalar function, $\vec{H}$ is an arbitrary vector function, V denotes a volume, ∂V denotes its surface, and $\vec{n}$ denotes the outward-directed unit normal associated with that surface. The vector $\vec{H}$ has the same mesh locations as the flux vector $\vec{F}$, but is

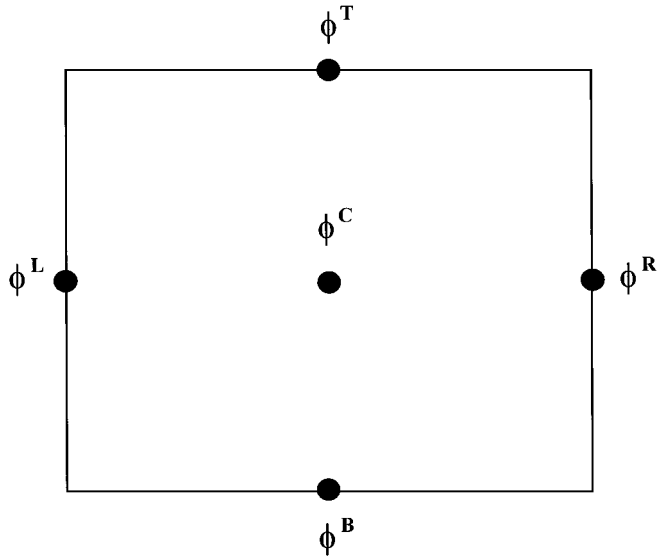

FIG. 3. Locations of intensity unknowns. The intensity unknowns are located at cell centers and face centers.

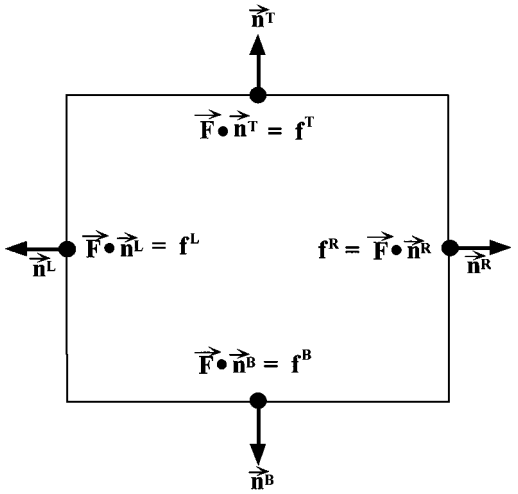

FIG. 4. Locations of vector component unknowns. One vector component is located at each face center and represents the dot product of the flux vector with the outward-directed face normal vector.

not necessarily equal to $-D\vec{\nabla}\phi$. We stress that the function ϕ at this point represents an arbitrary scalar function, and not necessarily the solution of the diffusion equation. The next step in our support-operators method is to discretize Eq. (5) over a single arbitrary cell in a special manner. Specifically, we explicitly discretize all but the modified gradient operator, which is expressed in an implicit form consistent with our choice of discrete unknowns. We assume indices of i, j for the arbitrary cell, but suppress these indices whenever possible in the discrete approximation to Eq. (5) that follows. We first discretize the surface integral,

$$\oint_{\partial V} \phi \vec{H} \cdot \vec{n}\, dA \approx \phi^R h^R A^R + \phi^B h^B A^B + \phi^L h^L A^L + \phi^T h^T A^T, \tag{6}$$

where A^R denotes the face area associated with the right face of the cell

$$A^R = 2\pi r_{i+\frac{1}{2}} \Delta z \tag{7}$$

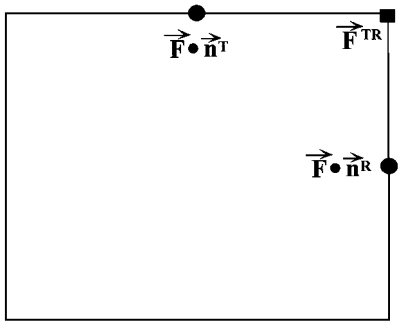

FIG. 5. Effective locations of complete flux vectors. Full flux vectors are considered to be located at cell corners and are composed of the components on the two faces associated with each corner. This is illustrated for the top-right corner vector, which is composed of the top-face and right-face flux components.

(the remaining face areas are defined analogously), and where

$$\Delta z = z_{j+\frac{1}{2}} - z_{j-\frac{1}{2}}. \tag{8}$$

Next we approximate the modified gradient volumetric integral,

$$\int_V -D^{-1}\vec{H}\cdot D\vec{\nabla}\phi\, dV \approx (D^{-1}\vec{H}^{RB}\cdot\vec{F}^{RB})V^{RB} + (D^{-1}\vec{H}^{BL}\cdot\vec{F}^{BL})V^{BL} + (D^{-1}\vec{H}^{LT}\cdot\vec{F}^{LT})V^{LT} + (D^{-1}\vec{H}^{TR}\cdot\vec{F}^{TR})V^{TR}, \tag{9}$$

where $\vec{F}$ denotes $-D\vec{\nabla}\phi$, and V^{RB} denotes the volumetric weight associated with the right-bottom corner,

$$V^{RB} = \frac{1}{4}\Delta r\,\Delta z\, 2\pi r_{i+\frac{1}{2}}, \tag{10}$$

$$\Delta r = r_{i+\frac{1}{2}} - r_{i-\frac{1}{2}}. \tag{11}$$

In analogy with Eq. (10), the volumetric weight associated with each corner consists of one-fourth the Cartesian cell volume multiplied by 2π times the value of the radius at that corner. These corner weights do not represent "true" volumes in any sense, but they do sum to the total cell volume,

$$V^{RB} + V^{BL} + V^{LT} + V^{TR} = V = \pi\left(r^2_{i+\frac{1}{2}} - r^2_{i-\frac{1}{2}}\right)\Delta z = 2\pi r_i\,\Delta r\,\Delta z, \tag{12}$$

where

$$r_i = \frac{1}{2}\left(r_{i-\frac{1}{2}} + r_{i+\frac{1}{2}}\right). \tag{13}$$

We choose these weights simply because they give us better properties than other more straightforward choices. The choice of weights is one of several free parameters in the support-operators method.

Finally, we approximate the divergence volumetric integral,

$$\int_V \phi\vec{\nabla}\cdot\vec{H}\, dV = \phi^C[h^R A^R + h^B A^B + h^L A^L + h^T A^T]. \tag{14}$$

Equations (6), (9), and (14) are certainly not unique, but they are fairly straightforward. For instance, Eq. (6) represents a face-centered second-order approximation to a surface integral. Equation (9) represents a corner-based volumetric integral consisting of a dot-product contribution from each pair of corner vectors. Equation (14) is a particularly simple second-order approximation which gives all of the weight to the cell-center value of ϕ while using a surface-integral formulation for $\vec{\nabla}\cdot\vec{H}$ that is analogous to the surface-integral used in Eq. (6).

Note that Eqs. (6), (9), and (14) define the discrete inner products discussed in [9]. Thus discretizing the fundamental integral identity expressed by Eq. (5) defines the discrete inner products associated with the adjoint relationship. We can now use this relationship to solve for the modified gradient operator components by substituting from Eqs. (6), (9), and (14) into Eq. (5) and requiring that the resulting discretized identity hold for *all* discrete $\vec{H}$ and ϕ values. More specifically, we obtain an equation for the modified gradient component on a

given face by setting the component of $\vec{H}$ on that face to unity while setting the components on all other faces to zero. For instance, setting $h^R = 1$, $h^B = 0$, $h^L = 0$, $h^T = 0$, we obtain an equation for f^R, which when solved yields

$$f^R = -\frac{2D}{\Delta r}(\phi^R - \phi^C). \tag{15}$$

Equation (15) represents a standard expression for f^R that is exact when ϕ is linearly dependent upon r. Similar expressions are obtained for the other face components. Substituting these expressions into the discrete volume-integrated divergence operator defined in Eq. (14) yields the discrete diffusion operator for a single cell,

$$\begin{aligned}\int_V -\vec{\nabla}\cdot D\vec{\nabla}\phi\, dV \approx &-\frac{2D}{\Delta r}[(\phi^R - \phi^C)A^R - (\phi^C - \phi^L)A^L] \\ &-\frac{2D}{\Delta z}[(\phi^T - \phi^C)A^T - (\phi^C - \phi^B)A^B].\end{aligned} \tag{16}$$

Combining expression (16) with standard point spatial discretizations for the time derivative and the source, we obtain the spatially discrete diffusion equation,

$$\begin{aligned}&V\frac{\partial}{\partial t}\phi^C - \frac{2D}{\Delta r}[(\phi^R - \phi^C)A^R - (\phi^C - \phi^L)A^L] \\ &-\frac{2D}{\Delta z}[(\phi^T - \phi^C)A^T - (\phi^C - \phi^B)A^B] = Q^C V.\end{aligned} \tag{17}$$

Equation (17) represents the equation for cell centers. To obtain the equations for the face-center intensities, we "connect" the cells in such a way that our discrete version of Eq. (5) holds over the entire mesh. It is not difficult to see that this requirement will be met if the surface integral in Eq. (5) is made to cancel between cells, resulting in a surface integral over the outer mesh boundary. This can be achieved by making the surface-normal fluxes and the intensities continuous across cell interfaces. For instance, considering the right face of cell i, j, we require that

$$\phi^R_{i,j} = \phi^L_{i+1,j}, \tag{18}$$

and that

$$f^R_{i,j} = -f^L_{i+1,j}. \tag{19}$$

Note that a $-$ occurs within Eq. (19) because the surface normals associated with $f^R_{i,j}$ and $f^L_{i+1,j}$ are opposite in sign. Enforcing continuity of the intensities leaves us with one intensity unknown at each face. Thus we can now uniquely refer to a face-center intensity in terms of its face-center index, i.e., the intensity at the right face of cell i, j and the left face of cell $i+1, j$ can now be uniquely referenced as $\phi_{i+1/2,j}$. In addition, we can now neglect the superscript C for the cell-center intensities. The continuity-of-flux equation at each cell face serves as the equation for the intensity at that face. However, to maintain both symmetry of the matrix and positive diagonal elements, we re-express Eq. (19) as

$$-A_{i+\frac{1}{2},j}\, f^R_{i,j} - A_{i+\frac{1}{2},j}\, f^L_{i+1,j} = 0, \tag{20}$$

where

$$A_{i+\frac{1}{2},j} = A^R_{i,j} = A^L_{i+1,j}. \tag{21}$$

Evaluating Eq. (20) in terms of the intensities, we obtain the equation for $\phi_{i+1/2,j}$,

$$\frac{A_{i+\frac{1}{2},j} 2D_{i,j}}{\Delta z_i}\left(\phi_{i+\frac{1}{2},j} - \phi_{i,j}\right) - \frac{A_{i+\frac{1}{2},j} 2D_{i+1,j}}{\Delta z_{i+1}}\left(\phi_{i+1,j} - \phi_{i+\frac{1}{2},j}\right) = 0. \tag{22}$$

The continuity-of-flux equation at an interface on the outer boundary of the grid is analogous to Eq. (20). However, there is only one real cell adjacent to the interface rather than two. The normal flux component associated with cell "outside" of the grid is given by an expression derived from the analytic boundary conditions. For instance, let us consider Eq. (20) evaluated at an interface on the right boundary of the mesh,

$$-A_{I+\frac{1}{2},j} f^R_{I,j} - A_{I+\frac{1}{2},j} f^L_{I+1,j} = 0, \tag{23}$$

where I denotes the maximum index of i. Cell $I+1, j$ does not exist, so we use the standard extrapolated boundary condition (standard in the radiation and neutron diffusion literature [1]) to obtain an expression for $f^L_{I+1,j}$. This condition takes the following form at the boundary,

$$\phi + d_e \vec{\nabla}\phi \cdot \vec{n} = \phi_e, \tag{24}$$

where d_e denotes the extrapolation distance, ϕ_e denotes the extrapolated intensity value, and $\vec{n}$ denotes the outward-directed unit normal vector. Note from Eq. (24) that this extrapolated condition is equivalent to a Robin or mixed condition. Recognizing that $D\vec{\nabla}\phi \cdot \vec{n}$ plays the role of $f^L_{I+1,j}$, we use Eq. (24) to obtain the desired expression for the "outside" flux component,

$$f^L_{I+1,j} = \frac{D_{i,j}}{d_e}\left(\phi_e - \phi_{i+\frac{1}{2},j}\right). \tag{25}$$

Using Eqs. (15), (23), and (25), we obtain the equation for $\phi_{I+1/2,j}$,

$$A_{I+\frac{1}{2},j}\left[\frac{2D_{I,j}}{\Delta z_I}\left(\phi_{I+\frac{1}{2},j} - \phi_{I,j}\right) - \frac{D_{I,j}}{d_e}\left(\phi_e - \phi_{I+\frac{1}{2},j}\right)\right] = 0. \tag{26}$$

A typical value for d_e is $2D$. This yields the Marshak boundary condition [1]. Note from Eq. (24) that if $d_e = 0$, one obtains the Dirichlet boundary condition with the boundary intensity given by ϕ_e. Furthermore, in the limit as $d_e \to \infty$, one obtains the Neumann condition.

Note from Eq. (22) that the continuity-of-flux equation for cell faces interior to the mesh relates the face-center intensity to the two adjacent cell-center intensities. Similarly note from Eq. (26) that the continuity-of-flux equation for faces on the outer boundary relates the face-center intensity to the only adjacent cell-center intensity and the extrapolated boundary intensity. Using these relationships to eliminate the face intensities from Eq. (16) results in the standard 5-point cell-center diffusion scheme. For instance, the following expression is obtained for the normal flux component on the right face of cell i, j,

$$f^R_{i,j} = -D_{i+\frac{1}{2},j}\frac{(\phi_{i+1,j} - \phi_{i,j})}{\Delta r_{i+\frac{1}{2}}}, \tag{27}$$

where

$$-D_{i+\frac{1}{2},j} = \left\{ \left(\frac{\Delta r_i}{D_i} + \frac{\Delta r_{i+1}}{D_{i+1}} \right) \frac{1}{\Delta r_i + \Delta r_{i+1}} \right\}^{-1}, \tag{28}$$

and

$$\Delta r_{i+\frac{1}{2}} = \frac{1}{2}(\Delta r_i + \Delta r_{i+1}). \tag{29}$$

Note that Eq. (27) contains only cell-center intensities. Further note that the definition for the face-center diffusion coefficient arises directly from the process of eliminating the face-center intensities. Thus we see that the method defines the face-center diffusion coefficient in terms of a specific averaging of the adjacent cell-center diffusion coefficients. In the case of a uniform mesh, this averaging reduces to the expected harmonic averaging. It is well known that the standard 5-point diffusion operator is symmetric positive-definite and has many other desirable properties.

3. THE QUADRILATERAL SCHEME

In this section we derive our new quadrilateral diffusion discretization scheme. The procedure is analogous to that for the orthogonal-mesh case. Note that the r and z coordinates carry full two-dimensional indices rather than the one-dimensional indices associated with an orthogonal mesh. A coordinate pair is assigned to each vertex in the mesh.

We again formulate a discrete approximation to Eq. (5). For the case of a general quadrilateral, the general form of the discrete surface integral is identical to Eq. (6). However, the expression for the face areas are slightly more complex than those of the orthogonal case. For instance,

$$A^R_{i,j} = 2\pi \left(\frac{r_{i+\frac{1}{2},j-\frac{1}{2}} + r_{i+\frac{1}{2},j+\frac{1}{2}}}{2} \right) \| \vec{r}_{i+\frac{1}{2},j+\frac{1}{2}} - \vec{r}_{i+\frac{1}{2},j-\frac{1}{2}} \|, \tag{30}$$

where

$$\vec{r} = (r, z), \tag{31}$$

and where the symbol $\| \cdot \|$ denotes the Euclidian vector norm. The other cell areas are defined in analogy with Eq. (30).

For the case of a general quadrilateral, the general form of the discrete modified gradient volumetric integral is identical to Eq. (9). However, there are two important differences in the definitions of certain quantities. First, since vectors are expressed in terms of normal surface components and the mesh is generally non-orthogonal, the dot product of two vectors cannot be taken in the standard way. For instance, in the orthogonal case, we can define the dot product in terms of the following inner product

$$\vec{H}^{TR} \cdot \vec{F}^{TR} = \langle \vec{H}^{TR}, \vec{F}^{TR} \rangle = h^T f^T + h^R f^R. \tag{32}$$

However, to take the dot product in the general non-orthogonal case, one must multiply either $\vec{H}$ or $\vec{F}$ by a particular SPD matrix, denoted by $\mathcal{S}$, before performing the inner

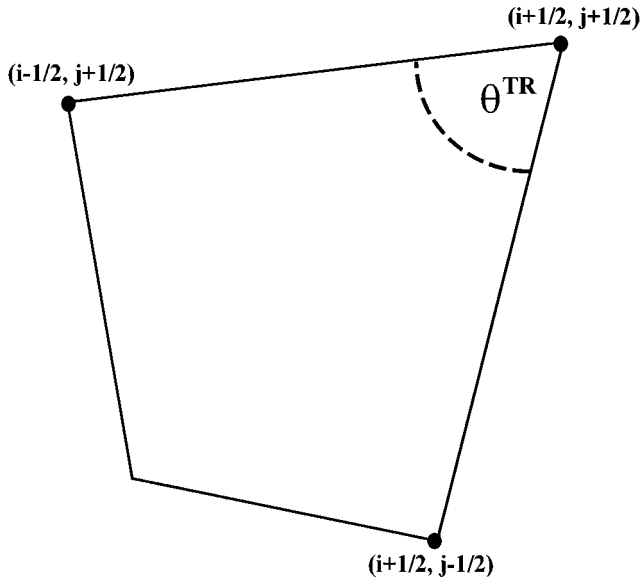

FIG. 6. *S*-matrix angle. The angle appearing in the *S*-matrix for the top-right corner is illustrated.

product,

$$\begin{aligned}\vec{H}^{TR}\cdot\vec{F}^{TR} &= \langle \mathcal{S}^{TR}\vec{H}^{TR}, \vec{F}^{TR}\rangle = \langle \vec{H}^{TR}, \mathcal{S}^{TR}\vec{F}^{TR}\rangle \\ &= s^{TR}_{T,T}h^T f^T + s^{TR}_{T,R}h^T f^R + s^{TR}_{R,T}h^R f^T + s^{TR}_{R,R}h^R f^R. \end{aligned} \tag{33}$$

The $\mathcal{S}$-matrix is completely defined by the angle formed by the sides of the corner asssociated with the two vector components. This angle is depicted in Fig. 6 for the top-right corner. In particular,

$$\mathcal{S}^{TR} = \frac{1}{\sin^2(\Theta^{TR})}\begin{bmatrix} 1 & \cos(\Theta^{TR}) \\ \cos(\Theta^{TR}) & 1 \end{bmatrix}. \tag{34}$$

Note that this matrix is invariant to the ordering of the surface-normal vector components. The $\mathcal{S}$-matrix is derived in Appendix A.

The second significant difference between the rectangular and quadrilateral cases arises in the volumetric weights assigned to each corner. In the orthogonal case, each corner weight is defined to be one-quarter of the cell area multiplied by 2π times the radius at that cell corner. For the quadrilateral case, we define each corner weight as one-quarter of the area defined by the parallelogram associated with that corner multiplied by 2π times the radius at that corner. The parallelogram associated with the top-right corner is illustrated in Fig. 7. The parallelograms associated with the other corners are analogously defined. Since these weights for the quadrilateral case do not necessarily sum to the total cell volume, we normalize them to ensure that they do so. For instance, the unnormalized volumetric weight for the top-right corner is given by

$$\tilde{V}^{TR} = \frac{1}{4}\left[\left(\vec{r}_{i-\frac{1}{2},j+\frac{1}{2}} - \vec{r}_{i+\frac{1}{2},j+\frac{1}{2}}\right)\cdot\left(\hat{r}_{i+\frac{1}{2},j-\frac{1}{2}} - \hat{r}_{i+\frac{1}{2},j+\frac{1}{2}}\right)\right]2\pi r_{i+\frac{1}{2},j+\frac{1}{2}}, \tag{35}$$

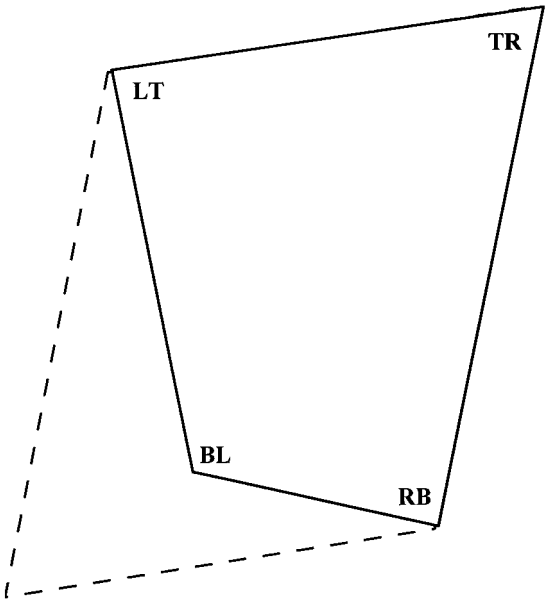

FIG. 7. Corner parallelogram. The parallelogram associated with the top-right corner of a quadrilateral overlays that quadrilateral.

where $\hat{r}$ denotes a right-handed 90-degree rotation of the vector $\vec{r} = (r, z)$:

$$\hat{r} = (z, -r). \tag{36}$$

The remaining volumetric weights are defined in analogy with Eq. (35). The normalized volumetric weight for the top-right corner is given by

$$V^{TR} = \tilde{V}^{TR} V / (\tilde{V}^{TR} + \tilde{V}^{RB} + \tilde{V}^{BL} + \tilde{V}^{LT}), \tag{37}$$

where V denotes the true volume of cell i, j,

$$\begin{aligned} V = &\left[\left(\vec{r}_{i-\frac{1}{2},j+\frac{1}{2}} - \vec{r}_{i+\frac{1}{2},j+\frac{1}{2}}\right)\cdot\left(\hat{r}_{i+\frac{1}{2},j-\frac{1}{2}} - \hat{r}_{i+\frac{1}{2},j+\frac{1}{2}}\right)\right]\frac{\pi}{3}\left(r_{i-\frac{1}{2},j+\frac{1}{2}} + r_{i+\frac{1}{2},j+\frac{1}{2}} + r_{i+\frac{1}{2},j-\frac{1}{2}}\right) \\ &+ \left[\left(\hat{r}_{i-\frac{1}{2},j+\frac{1}{2}} - \hat{r}_{i-\frac{1}{2},j-\frac{1}{2}}\right)\cdot\left(\vec{r}_{i+\frac{1}{2},j-\frac{1}{2}} - \vec{r}_{i-\frac{1}{2},j-\frac{1}{2}}\right)\right]\frac{\pi}{3}\left(r_{i+\frac{1}{2},j-\frac{1}{2}} + r_{i-\frac{1}{2},j-\frac{1}{2}} + r_{i-\frac{1}{2},j+\frac{1}{2}}\right). \end{aligned} \tag{38}$$

Note that all of the corner weights are multiplied by the normalization factor appearing in Eq. (37).

It would seem that more straightforward corner weights could be chosen that would not require renormalization. However, we found the choice of corner weights critical to obtaining certain important properties. In particular, we found no other choice of weights that gave us both second-order accuracy on non-smooth meshes and spherically symmetric solutions on spherically symmetric r-z meshes.

It is important to note that the expression given for the unnormalized corner weight in Eq. (35) gives a negative weight when the corner angle, Θ^{RT}, is greater than π. In this case, the cell is re-entrant and the corner volume is in fact negative. Negative weights can

result in a diffusion matrix that is not positive-definite. To avoid this difficulty, we simply substitute the absolute value of the corner volume for the true corner volume in Eq. (35):

$$\tilde{V}^{TR} = \frac{1}{4}\left|\left(\vec{r}_{i-\frac{1}{2},j+\frac{1}{2}} - \vec{r}_{i+\frac{1}{2},j+\frac{1}{2}}\right) \cdot \left(\hat{r}_{i+\frac{1}{2},j-\frac{1}{2}} - \hat{r}_{i+\frac{1}{2},j+\frac{1}{2}}\right)\right| 2\pi r_{i+\frac{1}{2},j+\frac{1}{2}}. \tag{39}$$

This procedure plays the role of the "parallelogram fixup" used in the MDHW scheme [6], but it is much simpler and just as effective.

For the case of a general quadrilateral, the general form of the discrete divergence volumetric integral is identical to that of Eq. (14). However, as previously noted for Eq. (6), the definition of the areas is given by Eq. (30) rather than Eq. (7).

To obtain expressions for the surface-normal components of the discrete gradient operator, we now proceed exactly as in the rectangular-mesh case. In particular, we first substitute from Eqs. (6), (9), and (14) (using the quadrilateral-mesh definitions for the components of these equations) into Eq. (5). Then we obtain an equation for the modified gradient component on each face by successively setting the component of $\vec{H}$ on a given face to unity while setting the components on all other faces to zero. In the rectangular-mesh case, four *independent* equations for the flux components are obtained. However, in the quadrilateral-mesh case, we obtain four *coupled* linear equations for the flux components that can be symbolically represented as

$$\mathcal{M}_a \vec{f} - \mathcal{M}_b \vec{\phi} = 0, \tag{40}$$

where

$$\vec{f} = (f^R, f^B, f^L, f^T), \tag{41}$$

$$\vec{\phi} = (\phi^R, \phi^B, \phi^L, \phi^T, \phi^C), \tag{42}$$

and where $\mathcal{M}_a$ is a 4×4 matrix and $\mathcal{M}_b$ is a 4×5 matrix. To obtain expressions for the flux components in terms of the intensities, one need simply invert $\mathcal{M}_a$ and apply it to $\mathcal{M}_b$,

$$\vec{f} = \mathcal{F}\vec{\phi}, \tag{43}$$

where $\mathcal{F} = \mathcal{M}_a^{-1}\mathcal{M}_b$. Because $\mathcal{M}_a$ is nearly full, we choose to invert it numerically. Unfortunately, this means that we cannot give explicit expressions for the flux components in the quadrilateral-mesh case. Nonetheless, a useful constructive expression for $\mathcal{F}$ is given in Eq. (71) in Appendix B.

It can be shown that $\mathcal{M}_a$ is non-singular as long as the quadrilateral is not degenerate, i.e., as long as it does not have coincident vertices or corner angles equal to 180 degrees. Nonetheless, solutions can be obtained for degenerate cases simply by taking appropriate limits. For instance, equations for triangles are easily obtained. A triangle is viewed as a quadrilateral with one face of zero area. The unknowns associated with such a degenerate face completely decouple from the other unknowns, allowing one to arbitrarily define the degenerate unknowns while leaving the other unknowns unaffected.

The conditions for connecting cells are identical to those of the orthogonal case: continuity of intensity and flux across cell interfaces. Continuity of the intensity leads to a unique intensity at each cell face. The equation for each face-center intensity expresses the continuity of flux. For the quadrilateral case, the flux-continuity equation has the same

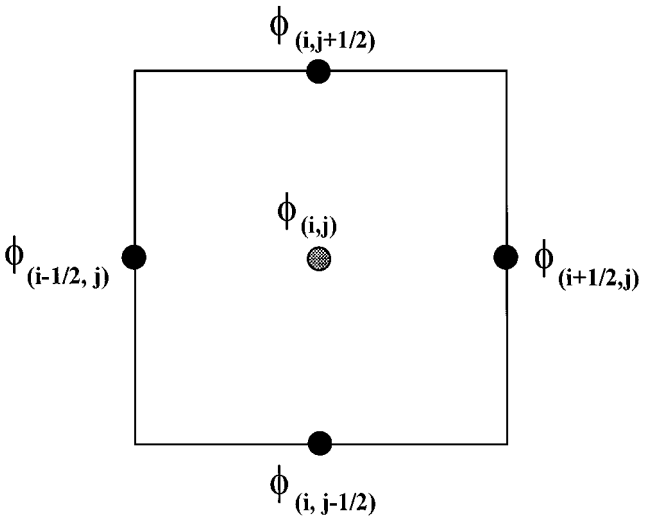

FIG. 8. Stencil for the cell-center intensity at mesh location (i, j).

general from as Eq. (20), but the area elements are given by Eq. (30) rather than Eq. (7), and the modified gradient components are given by Eq. (43) rather than Eq. (15). Since the extrapolated boundary condition given in Eq. (24) is analytic, it can be applied to quadrilaterals as well as rectangles to obtain the normal flux component on a boundary face. For instance, Eq. (25) is valid on both rectangles and quadrilaterals. The point discretizations for the time derivative and source terms used in Eq. (17) are also used in the quadrilateral case. This completes the specification of our quadrilateral-mesh scheme.

As previously demonstrated, the face-center intensities on a rectangular mesh can be eliminated via the continuity-of-flux equations to obtain a 5-point cell-center diffusion scheme. Unfortunately, in the quadrilateral case this process yields a cell-center diffusion scheme that has a full coefficient matrix. This is the *same* cell-center scheme that one would obtain by applying the standard support-operators method of Shashkov and Steinberg [9] in conjunction with our definitions for the discrete inner products.

Our quadrilateral scheme yields a 5-point stencil for the cell-center equations and a 9-point stencil for the face-center equations. The stencil for the cell-center intensity at mesh location (i, j) is illustrated in Fig. 8. The stencil for the face-center intensity at mesh location $i, j + \frac{1}{2}$ is illustrated in Fig. 9.

Although we do not consider tensor diffusion in this paper, the local support-operators formalism which we have described readily admits such diffusion as long as the diffusion tensor is SPD. In particular, the discretizations for Eq. (5), given in Eqs. (6), (9), and (14), remain valid with an SPD tensor diffusion coefficient. In the quadrilateral case, one need simply ensure that D and D^{-1} are transformed from the standard Cartesian basis to the appropriate surface-normal basis.

4. SOLUTION OF THE EQUATIONS

We use a multigrid-preconditioned conjugate-gradient [13] method to solve our discrete diffusion equation. The preconditioner is based upon an approximate 5-point cell-center diffusion operator. As previously discussed, our cell-center/face-center system of equations

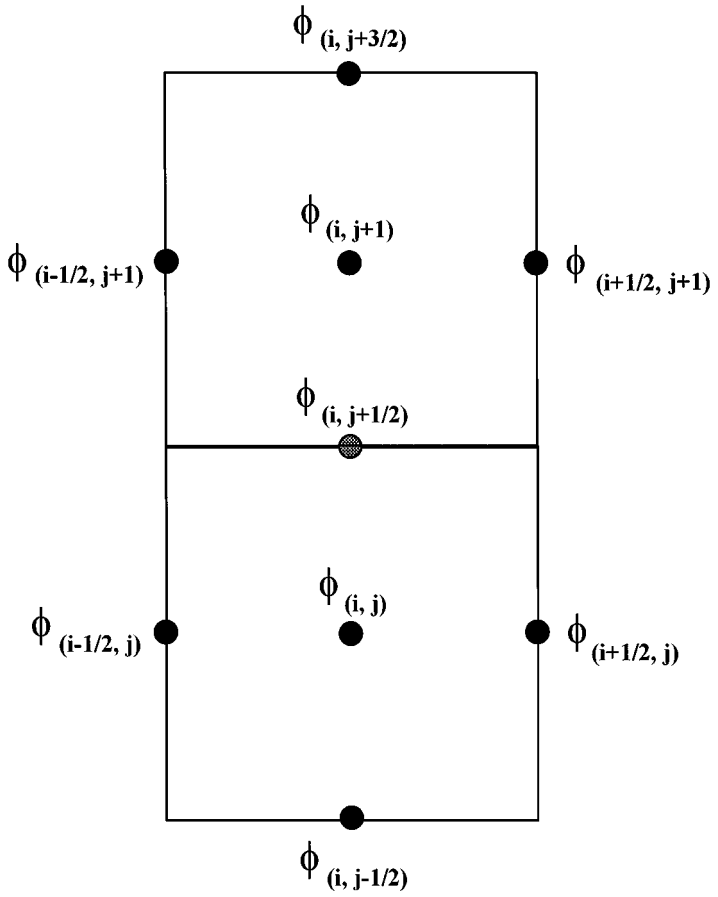

FIG. 9. Stencil for the face-center intensity at mesh location $(i,\ j+\frac{1}{2})$.

can be reduced to a 5-point cell-center system when the mesh is orthogonal by eliminating the face-center intensities. This is possible whenever the corner S-matrices are diagonal. However, they are rigorously diagonal only when the mesh is orthogonal. We obtain our approximate cell-center system simply by first setting the off-diagonal elements of the corner S-matrices to zero, and then eliminating the face-center unknowns. In the preconditioning step, we do not fully solve this approximate system, but rather perform a set number of V-cycles using Dendy's black-box multigrid algorithm [14]. When the mesh is orthogonal, the "approximate" system is actually exact, but as the mesh becomes increasingly skewed, it becomes less accurate. Nonetheless, as shown in the next section, this method performs extremely well on moderately skewed meshes and fairly well on highly skewed meshes.

It is useful to consider certain details which arise when deriving and solving our approximate cell-center operator. Let us assume that our full cell-center/face-center equations are expressed in terms of the matrix equation

$$\mathcal{M}\vec{\phi} = \vec{q}, \tag{44}$$

where $\mathcal{M}$ is the coefficient matrix, $\vec{\phi}$ is the solution vector, and $\vec{q}$ is the source vector. The

preconditioning step in the conjugate-gradient method consists of solving a matrix equation of the form [13]

$$\tilde{\mathcal{M}}\overrightarrow{\delta\phi} = \overrightarrow{\delta q}, \tag{45}$$

where $\tilde{\mathcal{M}}$ denotes the approximation to $\mathcal{M}$ (called the preconditioner) and $\overrightarrow{\delta q}$ denotes a residual. The matrix appearing in Eq. (45) consists of the full cell-center/face-center system modified with the diagonal approximation for the corner $\mathcal{S}$-matrices. As can be seen from Eq. (20), the face-center (continuity of flux) equations associated with our scheme normally do not contain sources. However, the face-center equations associated with Eq. (45) will have sources arising from the residual vector. Thus when the 5-point cell-center preconditioning system is derived from Eq. (45) by eliminating the face-center components of $\overrightarrow{\delta\phi}$, one must include the face-center residual components in the elimination process. Furthermore, after the V-cycles have been carried out to obtain the cell-center components of $\overrightarrow{\delta\phi}$, one must use these components together with the face-center equations to calculate the face-center components of $\overrightarrow{\delta\phi}$.

5. COMPUTATIONAL RESULTS

In this section we present computational results which demonstrate the accuracy of our method and the efficiency of our solution technique. The method of Morel, Dendy, Hall, and White (MDHW) was computationally compared with several existing cell-centered Lagrangian-mesh diffusion differencing schemes in [6]. The accuracy of this method was clearly superior to that of the other schemes, but it was also significantly more expensive. Our scheme has the same unknowns as the MDHW scheme, the same cell-center stencil, and nearly the same face-center stencil (our scheme has a 9-point face-center stencil while the MDHW scheme has a 7-point face-center stencil). Nonetheless, our method is less expensive than the MDHW scheme because we use conjugate-gradient iterations rather than fine-mesh line relaxations to solve our equations. The cost of solving the MDHW equations is dominated by the cost of performing such relaxations. We are able to use the conjugate-gradient solution technique because our coefficient matrix is SPD. The MDHW equations cannot be solved with the conjugate-gradient technique because the MDHW scheme has an asymmetric coefficient matrix.

We have performed many of the calculations that appear in [6], but we have also performed several calculations relating to the convergence of our scheme on spherical meshes. The first set of calculations that we performed relate to the accuracy of our scheme on highly skewed mesh. We consider the Kershaw-mesh problem given in [6]. A 10×10 Kershaw mesh is shown in Fig. 10. The following equation was solved,

$$-\frac{1}{r}\frac{\partial}{\partial r}\left[rD\frac{\partial\phi}{\partial r}\right] - \frac{\partial}{\partial z}\left[D\frac{\partial}{\partial z}\phi\right] = 0, \tag{46}$$

for $r \in [0, 1]$, $z \in [0, 1]$. The problem has reflective boundaries along $r = 0$ and $r = 1$, a Marshak vacuum boundary along $z = 1$, and a unit extrapolated Marshak boundary condition along $z = 0$. The solution to this problem is a linear function of z [6]. Although the MDHW scheme yields the exact solution to this problem, our scheme does not. We were unable to define inner product weights that would enable our method to yield exact linear

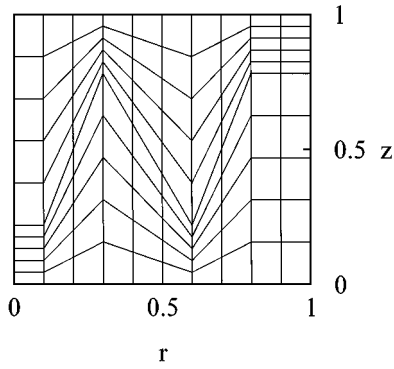

FIG. 10. The 10×10 Kershaw mesh.

homogeneous solutions while maintaining all the other desirable properties of our scheme. Nonetheless, one would expect our scheme to converge to the exact solution as the mesh is refined. The intensity contours for the 10×10 mesh using our support-operators method are shown in Fig. 11. The exact contours are constant in r, but the support-operators contours are not constant. Rather they show some mesh distortion. However, the same calculation was repeated with a 48×48 mesh. This mesh is shown in Fig. 12. The corresponding intensity contours are shown in Fig. 13. The contours appear to be constant in r. This demonstrates the convergence of our method on highly shewed meshes.

The second set of calculations addresses the accuracy of our method on highly distorted meshes with re-entrant cells. We solve the same basic problem for the second set of calculations that was solved for the first set of calculations. A single calculation is performed on the 32×32 Shestakov mesh referred to in [6]. This mesh is shown in Fig. 14. It is clearly both highly skewed and highly distorted. It contains several cells that are re-entrant, and thus have negative corner volumes. For such cases, we substitute the absolute value of the negative weight, and then renormalize all four of the cell weights so that they sum to the correct volume. This is the analogue of the "parallelogram fixup" defined for the MDHW scheme. However, the support-operators "fixup" is much simpler, just as effective, and does not have to be implemented as often as the MDHW fixup. The intensity contours are shown in Fig. 15. These contours are nearly constant in r. This represents a very good result considering the fact that some of the cells are re-entrant.

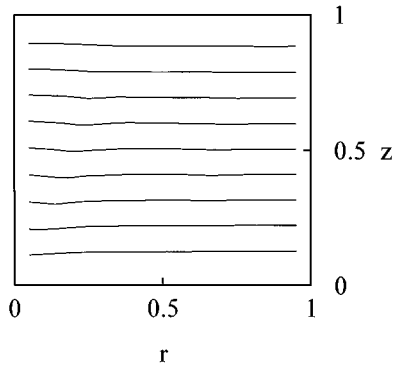

FIG. 11. Intensity contours for the 10×10 Kershaw mesh. The exact contours are constant in r.

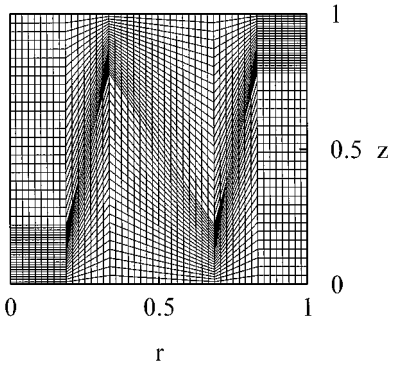

FIG. 12. The 48 × 48 Kershaw mesh.

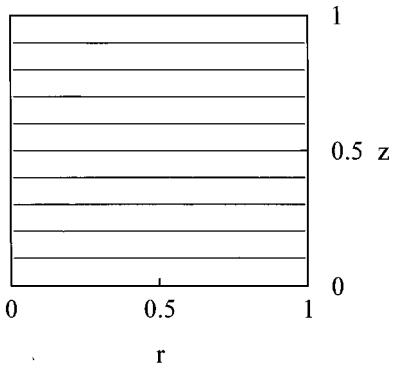

FIG. 13. Intensity contours for the 48 × 48 Kershaw mesh. The exact contours are constant in r.

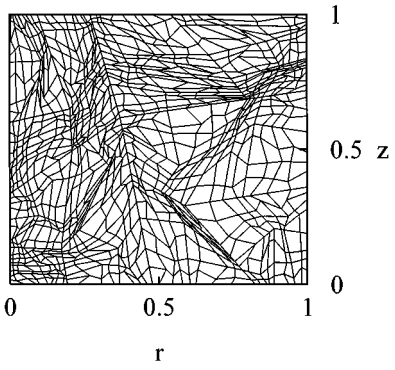

FIG. 14. The 32 × 32 Shestakov mesh.

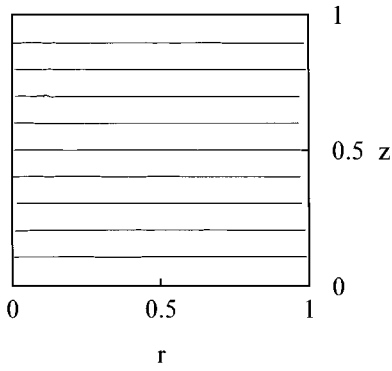

FIG. 15. Intensity contours for the 32×32 Shestakov mesh. The exact contours are constant in r.

The third set of calculations addresses the convergence of our method on grids that are mildly distorted. Cylindrical random grids were used for similar purposes in [6]. We have used spherical random grids to demonstrate that our method converges on meshes containing triangles as well as quadrilaterals. These random grids were generated by moving each mesh vertex to a random position on a circle centered about the original vertex position. The radius of each circle was roughly one-fifth of the cell width. The 2-D r-z equivalent of the following 1-D equation was solved,

$$-\frac{1}{R^2}\frac{\partial}{\partial R}\left[R^2 D\frac{\partial \phi}{\partial R}\right] = a + bR^2, \tag{47}$$

for $R \in [0, 1]$, where R denotes the spherical radius, i.e., $R = \sqrt{r^2 + z^2}$, D denotes a region-dependent diffusion coefficient, and $a = b = 1$. The problem domain consists of a two-region sphere illustrated in Fig. 16. The inner region is defined by $0 < R < 0.5$, and the outer region is defined by $0.5 < R < 1.0$. The diffusion coefficient is 1 in the inner region and 2 in the outer region. There are reflective boundary conditions along $z = 0$ and $r = 0$, and a Marshak vacuum boundary condition along $R = 1$. The analytic solution to this problem is

$$\phi_1 = a\left(\frac{1}{3} + \frac{1}{24D_1} + \frac{1}{8D_2}\right) + b\left(\frac{2}{5} + \frac{1}{320D_1} + \frac{3}{64D_2}\right) - \frac{aR^2}{6D_1} - \frac{bR^4}{20D_1}, \tag{48}$$

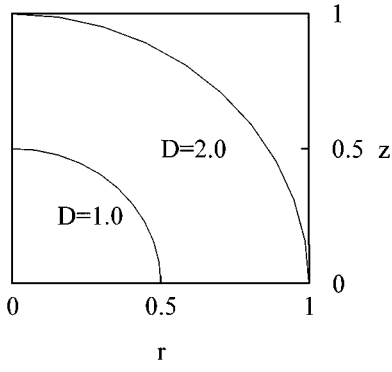

FIG. 16. Spherical test problem domain.

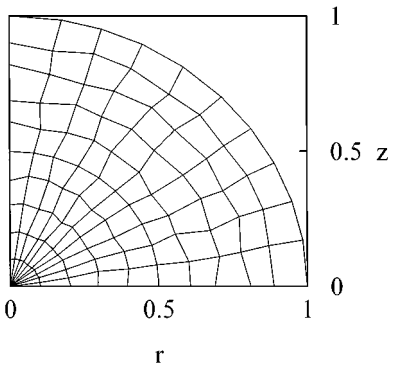

FIG. 17. The 10×10 random spherical mesh. Note that the interface between material regions is not distorted.

$$\phi_2 = a\left(\frac{1}{3} + \frac{1}{6D_2}\right) + b\left(\frac{2}{5} + \frac{1}{20D_2}\right) - \frac{aR^2}{6D_2} - \frac{bR^4}{20D_2}, \tag{49}$$

where ϕ_1 and ϕ_2 respectively denote intensity solutions in the inner and outer regions, and D_1 and D_2 similarly denote the diffusion coefficients in the inner and outer regions.

Calculations were performed using our scheme on several randomly distorted grids. For instance, a 10×10 spherical random grid is shown in Fig. 17 and a 20×20 spherical random grid is shown in Fig. 18. The relative L_2 error norm is plotted in Fig. 19 for each calculation as a function of radial cell width. This relative norm consists of the standard L_2 norm of the cell-center intensity errors divided by the L_2 norm of the exact cell-center intensity solution. The error dependence expected with second-order convergence is also plotted in Fig. 19. The computed errors clearly agree with the expected errors, indicating that our scheme is second-order accurate on these randomly distorted spherical meshes that contain both a material discontinuity and triangular cells.

The fourth set of calculations is primarily intended to address the accuracy of our scheme relative to the MDHW scheme as a function of the mesh distortion. We performed calculations for a problem defined in [6]. The following equation was solved,

$$-\frac{1}{r}\frac{\partial}{\partial r}\left[rD\frac{\partial \phi}{\partial r}\right] - \frac{\partial}{\partial z}\left[D\frac{\partial \phi}{\partial z}\right] = qz^2, \tag{50}$$

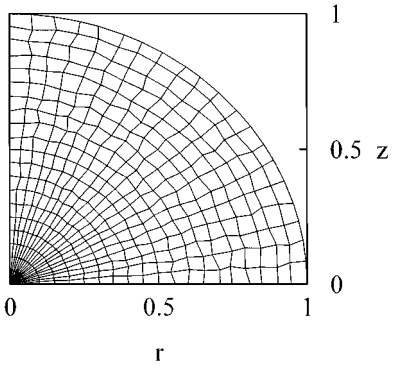

FIG. 18. The 20×20 random spherical mesh. Note that the interface between material regions is not distorted.

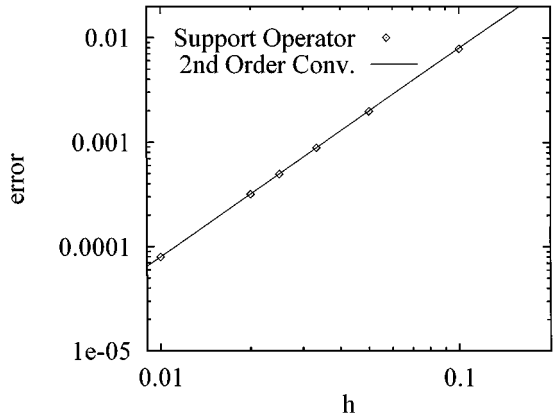

FIG. 19. Error versus radial cell width.

for $r \in [0, 1]$, $z \in [0, 1]$, where q is a constant. There are reflective boundary conditions along $r = 0$ and $r = 1$, and Marshak vacuum boundaries along $z = 0$ and $z = 1$. The diffusion coefficient has a value of unity throughout the problem. The analytic solution to this problem is

$$\phi = a + bz + cz^4, \tag{51}$$

where

$$a = \frac{q}{6}\left[\frac{1+8D}{1+4D}\right], \tag{52}$$

$$b = \frac{q}{12D}\left[\frac{1+8D}{1+4D}\right] \tag{53}$$

$$c = -\frac{q}{12D}. \tag{54}$$

We have computed the solution to this problem using our support-operators scheme and the MDHW scheme on a 48×48 orthogonal mesh, a 48×48 random mesh, a 48×48 Kershaw mesh, and a 32×32 Sheshtakov mesh. The relative L_2 errors for these calculations are given in Table 1. The support-operators and MDHW methods give the same error on the orthogonal mesh because they are identical on such meshes. They give comparable errors on all of the other meshes. This is similar to the results obtained by Steinberg and Shashkov when comparing their support-operators method with the MDHW method in x-y geometry [9].

We also used the fourth set of calculations to compare the iterative convergence rate of our multigrid-preconditioned conjugate-gradient solution technique with the MDHW

TABLE 1
Comparison of Support-Operators and MDHW Accuracy

Mesh	SO error	MDHW error
48×48 orthogonal	4.72×10^{-5}	4.72×10^{-5}
48×48 random	4.31×10^{-5}	4.38×10^{-5}
48×48 Kershaw	2.23×10^{-4}	2.19×10^{-4}
32×32 Shestakov	6.78×10^{-4}	7.50×10^{-4}

TABLE 2
Iterative Convergence Comparison of Support-Operators and MDHW Schemes

Mesh	SO iterations	MDHW iterations
48×48 orthogonal	3	6
48×48 random	11	8
48×48 Kershaw	59	84
32×32 Shestakov	94	50

multigrid solution technique. The iterations required to converge the support-operators and multigrid solution techniques are given in Table 2. The solutions were considered converged when the L_2 norm of the residual vector divided by the L_2 norm of the source vector was less than 10^{-6}. It can be seen from Table 2 that mixed results were obtained. In two cases the support-operators scheme took fewer iterations and in two other cases the MDHW scheme took fewer iterations. Neither scheme ever took more than twice the iterations required by the other. A direct timing comparison between these two methods is difficult because the support-operators and MDHW calculations had to be performed on different computers (a SUN workstation and a CRAY-YMP, respectively.) Nonetheless, we can make some rough quantitative statements about the relative costs of these two schemes based upon the following information. The fraction of the total solution time spent in conjugate gradient iterations was roughly 0.33 for the support-operators method, and the fraction of the total solution time spent in line relaxation iterations was roughly 0.83 for the MDHW method. The support-operators and MDHW solution techniques significantly differ only in that the support-operators scheme uses a conjugate-gradient iteration in place of the line relaxations used in the MDHW scheme. The multigrid component of these two methods is essentially identical. Given this fact, it follows from these time fractions that a line relaxation iteration is roughly an order of magnitude more costly than a conjugate-gradient iteration. Furthermore, it follows that the support-operators method should be roughly 4 times faster per iteration than the MDHW method on the same computer. Since the MDHW scheme never takes less than half the iterations taken by the support-operators method, it follows that the support-operators method should never be less than 2 times faster than the MDHW scheme on the same computer. It is not our purpose to make a detailed quantitative comparison of the efficiency of these schemes for a large class of problems. Rather we simply seek to demonstrate that our support-operators scheme can be expected to be significantly faster than the MDHW scheme for problems similar to those modeled in our calculations.

It is important to note from Table 2 that the iterative convergence rates for both our support-operators method and the MDHW method degrade as the mesh becomes increasingly distorted. This is not surprising since both methods use an approximate 5-point cell-center diffusion operator to improve the convergence rate, and these operators are highly inaccurate on distorted meshes. This degradation of our preconditioner is perhaps the most significant deficiency of our solution technique. There is clearly much room for improvement in the preconditioner.

In closing this section, we consider the cost of our support-operators scheme relative to a cell-center diffusion scheme. Since our scheme has both cell-center and face-center unknowns, it is clear that it must be significantly more expensive than a pure cell-center scheme. In general, one should compare two discretization schemes in terms of accuracy per

unit computational cost. However, such a comparison is somewhat ill-posed for the case we are considering because, to our knowledge, all cell-center finite-difference schemes with sparse diffusion matrices are non-convergent for certain classes of realistic problems on well-behaved but non-smooth meshes. Thus for certain problems, the desired accuracy may only be attainable with our method.

Let us consider a 9-point cell-center diffusion scheme that is being solved using the conjugate gradient technique in conjunction with multigrid preconditioning. Since our scheme has as 9-point stencil for the face-center equations and a 5-point stencil for the cell-center equations, the average bandwidth of our scheme is a little less than 8. The cost of a matrix-vector multiplication is roughly proportional to the length of the vector times the matrix bandwidth, and the cost of a dot product is proportional to the vector length. The work associated with a conjugate-gradient iteration (neglecting the preconditioning component) is dominated by matrix-vector multiplication and dot products. Thus if we neglect the multigrid preconditioning step, the cost per conjugate-gradient iteration of our support-operators method should be no more than about 3 times that of a 9-point cell-center scheme. The multigrid preconditioning step would be fairly similar for both schemes except that our scheme would require the additional step of solving for the face-center unknowns in the preconditioning equation once the cell-center unknowns have been obtained from the multigrid V-cycle.

6. SUMMARY AND FUTURE WORK

We have developed a new "local" version of the support-operators method and applied it to the discretization of the diffusion operator on quadrilateral meshes. This local scheme yields a sparse banded diffusion matrix in contrast to the standard support-operators approach of Shashkov and Steinberg [9], which yields a dense diffusion matrix. However, the local approach requires face-center intensity unknowns in addition to the cell-center intensity unknowns, and thus is more costly than pure cell-center schemes. The additional cost is roughly a factor of 3 in both memory and CPU time per iteration. This is clearly a significant increase in cost, but our support-operators scheme yields a sparse banded symmetric positive-definite diffusion matrix, and converges with second-order accuracy even on grids that are not smooth and contain material discontinuities. We are unaware of any cell-center finite-difference scheme that has these properties. In addition, our scheme conserves energy over each spatial cell, yields spherically symmetric solutions on spherically symmetric r-z grids, and is sufficiently robust to provide a conservative solution even on meshes that contain re-entrant cells, e.g., boomerang and bowtie cells [6]. The only restriction on the re-entrant cells is that they must have a positive total volume. We believe that this highly desirable set of properties more than justifies the additional cost of our scheme.

In the future we intend to investigate the solution of the system which results from eliminating the cell-center intensity unknowns in our equations. This could reduce the CPU time associated with our scheme by a third. We also intend to investigate new approximate diffusion discretizations for preconditioning our support-operators equations. Our intent is to find a preconditioner that suffers less degradation as the mesh becomes increasingly distorted. An obvious candidate would be a 9-point cell-center discretization. Finally, we intend to investigate the generalization of our quadrilateral-mesh method to 3-D hexahedral meshes.

APPENDIX A

In this appendix we derive the matrix S that is defined in Eq. (34). We begin by considering the top-right corner of the quadrilateral shown in Fig. 6. The flux vector associated with this corner is expressed in terms of its components with respect to the top-face and right-face normals:

$$\vec{F} = (\vec{F} \cdot \vec{n}^T, \vec{F} \cdot \vec{n}^R) = (f^T, f^R). \tag{55}$$

Note that the superscript "TR" for the vector $\vec{F}$ has been suppressed in Eq. (55) for simplicity. It is trivial to relate the standard r and z components of $\vec{F}$ to the normal components. In particular,

$$G\bar{F} = \vec{F}, \tag{56}$$

where

$$G = \begin{bmatrix} n_r^T & n_z^T \\ n_r^R & n_z^R \end{bmatrix}, \tag{57}$$

$$\bar{F} = \begin{bmatrix} f_r \\ f_z \end{bmatrix}, \tag{58}$$

$$\vec{F} = \begin{bmatrix} f^T \\ f^R \end{bmatrix}, \tag{59}$$

and where a subscript r denotes an r-component and a subscript z denotes a z-component. The vector $\bar{F}$ is said to be in the r-z basis, while the vector $\vec{F}$ is said to be in the face-normal basis. Inverting G in Eq. (56), we get

$$\bar{F} = G^{-1}\vec{F}. \tag{60}$$

By definition, the dot product of any two r-z basis vectors, $\bar{F}$ and $\bar{H}$, is given by

$$\bar{F} \cdot \bar{H} = f_r h_r + f_z h_z. \tag{61}$$

It follows from Eqs. (60) and (61) that

$$\bar{F} \cdot \bar{H} = G^{-1}\vec{F} \cdot G^{-1}\vec{H}, \tag{62}$$

where $\vec{H}$ is the face-normal counterpart of $\bar{H}$. Using the inner product defined in Eq. (32), we can re-express Eq. (62) as

$$\begin{aligned} \bar{F} \cdot \bar{H} &= \langle \vec{F}, [G^{-1}]^t G^{-1}\vec{H} \rangle \\ &= \langle [G^{-1}]^t G^{-1}\vec{F}, \vec{H} \rangle, \end{aligned} \tag{63}$$

where a superscript "t" denotes the matrix transpose. Comparing Eqs. (33) and (63), it is evident that

$$\mathcal{S}^{TR} = [G^{-1}]^t G^{-1}. \tag{64}$$

Equation (34) can be obtained from Eqs. (57) and (64) after tedious but straightforward algebraic manipulations.

APPENDIX B

In this appendix we demonstrate that the coefficient matrix which arises from our discretization method is Symmetric Positive Definite (SPD). For simplicity, we ignore the contributions from the time-derivative term in Eq. (1). If standard temporal differencing (e.g., fully implicit or Crank–Nicholson) is used, this term will not affect the positive-definite character of the matrix because it contributes only to the diagonal elements.

Before we begin the demonstration we need to prove that the null space of a sum of matrices having Cholesky decompositions is the intersection of the null spaces of the individual matrices. For each value of the integer c, let $\mathcal{M}_c$ denote a matrix that has a Cholesky decomposition, and let $\mathcal{M}$ denote the sum over all c of these matrices,

$$\begin{aligned}\mathcal{M} &= \sum_c \mathcal{M}_c, \\ &= \sum_c \mathcal{L}_c \mathcal{L}_c^t, \end{aligned} \tag{65}$$

where $\mathcal{L}_c$ is a real lower triangular matrix with non-negative diagonals. The inner product of $\mathcal{M}$ with a vector x is then

$$\begin{aligned} x^t \mathcal{M} x &= \sum_c x^t \mathcal{M}_c x, \\ &= \sum_c x^t \mathcal{L}_c \mathcal{L}_c^t x, \\ &= \sum_c y_c^t y_c, \\ &\geq 0. \end{aligned} \tag{66}$$

The only way the equality can be satisfied is if each term in the sum is itself equal to zero, and therefore each y_c is the zero vector. This implies that x is in the null space of every $\mathcal{M}_c$ since

$$\begin{aligned} \mathcal{M}_c x &= \mathcal{L}_c \mathcal{L}_c^t x, \\ &= \mathcal{L}_c y_c, \\ &= 0. \end{aligned} \tag{67}$$

In addition Eq. (66) demonstrates that $\mathcal{M}$ is Symmetric Positive Semidefinite (SPS). If the intersection of the null spaces are the empty set then the inequality in Eq. (66) becomes strictly greater, and $\mathcal{M}$ is SPD.

Our demonstration proceeds as follows. First we consider the matrix equation for a single-cell mesh with Neumann boundary conditions, and show that it has a Cholesky decomposition. Next we show that the matrix for a multi-cell mesh with reflective conditions on the outer boundary faces can be constructed from single-cell matrices, and use this fact to

determine the null space of the multi-cell matrix. Any well-posed steady-state problem must include at least one outer boundary face with a Dirichlet or extrapolated boundary condition (see Eq. (24)). Without loss of generality, we consider only the extrapolated condition. We next show that the multi-cell matrix becomes SPD when the Neumann condition at one or more boundary faces is replaced with an extrapolated boundary condition. In particular, we show that the extrapolated boundary condition reduces the null space of the matrix to the empty set.

Before proceeding, there are several natural assumptions that must be made about the mesh. The first is that the corner weights defined by Eq. (37) are positive. The second assumption is that all of the face areas defined by Eq. (30) are positive. All of these assumptions are valid if the quadrilaterals are non-degenerate. Our diffusion matrix is also SPD with certain types of degenerate cells, e.g., triangles, but we do not consider such cells here.

We begin the demonstration by constructing the matrix equation for a single-cell mesh with Neumann conditions. This requires the definition and construction of several constituent matrices. For instance, consider the matrix formed by the weighted sum of the S-matrices defined in Eq. (34):

$$\mathcal{S} = V^{TR}\mathcal{S}^{TR} + V^{RB}\mathcal{S}^{RB} + V^{BL}\mathcal{S}^{BL} + V^{TL}\mathcal{S}^{LT}. \tag{68}$$

Under the assumptions previously described, $\mathcal{S}$ is a real 4×4 SPD matrix, as is its inverse, $\mathcal{S}^{-1}$. These matrices operate on the space of real 4-vectors representing the surface-normal flux components: $\vec{f} = (f^R, f^B, f^L, f^T)$. Next we define two matrices that are constructed from the face areas,

$$\mathcal{A} = \begin{bmatrix} A^R \\ A^B \\ A^L \\ A^T \end{bmatrix} \in \mathcal{R}^{4\times 1}, \tag{69}$$

$$\mathcal{W} = \begin{bmatrix} A^R & 0 & 0 & 0 \\ 0 & A^B & 0 & 0 \\ 0 & 0 & A^L & 0 \\ 0 & 0 & 0 & A^T \end{bmatrix} \in \mathcal{R}^{4\times 4}. \tag{70}$$

These matrices can be used to define the fundamental matrix, $\mathcal{F}$, which expresses the flux componments in terms of the intensities,

$$\begin{aligned} \vec{f} &= \mathcal{F}\vec{\phi}, \\ &= [\mathcal{F}_1, \mathcal{F}_2]\vec{\phi}, \\ &= D\mathcal{S}^{-1}[-\mathcal{W}, \mathcal{A}]\vec{\phi}, \end{aligned} \tag{71}$$

where $\vec{\phi} = (\phi^R, \phi^B, \phi^L, \phi^T, \phi^C)$. Note that $\mathcal{F}$ is a 4×5 real matrix expressed in block form. The first block operates off the face-center intensities and the second block operates on the cell-center intensity.

The equation for the cell-center intensity corresponds to a statement of energy conservation over the cell,

$$\oint_{\partial V} \vec{F} \cdot \hat{n}\, dA = \int_V Q\, dV. \tag{72}$$

In discrete form, this equation is

$$A^R f^R + \cdots + A^T f^T = Q^C V, \tag{73}$$

where V denotes the cell volume. This equation can be expressed as

$$\mathcal{A}^t \mathcal{F} \vec{\phi} = Q^C V. \tag{74}$$

The equations for the face-center intensities arise from the Neumann boundary condition at each face of the cell. In particular, each surface-normal flux component must be zero. To achieve symmetry, we express this requirement as follows for the right-face intensity:

$$-A^R f^R = 0. \tag{75}$$

The equations for the other face-center intensities are analogous. The equations for all of the face-center intensities can be expressed as

$$-\mathcal{W}\mathcal{F}\vec{\phi} = \vec{0}, \tag{76}$$

where $\vec{0}$ is a 4-vector.

Using Eqs. (74) and (76), we can construct the matrix equation for the intensities on a single-cell mesh with Neumann boundary conditions:

$$\mathcal{M}_5 \vec{\phi} = \begin{bmatrix} -\mathcal{W}\mathcal{F} \\ \mathcal{A}^t \mathcal{F} \end{bmatrix} \vec{\phi} = D \begin{bmatrix} \mathcal{W}\mathcal{S}^{-1}\mathcal{W} & -\mathcal{W}\mathcal{S}^{-1}\mathcal{A} \\ -\mathcal{A}^t\mathcal{S}^{-1}\mathcal{W} & \mathcal{A}^t\mathcal{S}^{-1}\mathcal{A} \end{bmatrix} \vec{\phi} = \begin{bmatrix} \vec{0} \\ Q^C V \end{bmatrix}. \tag{77}$$

We now begin a demonstration that the matrix $\mathcal{M}_5$ has a Cholesky decomposition. Because the matrix $\mathcal{S}^{-1}$ is SPD, it can be expressed as

$$\mathcal{S}^{-1} = \mathcal{L}_\mathcal{S} \mathcal{L}_\mathcal{S}^t, \tag{78}$$

where $\mathcal{L}_\mathcal{S}$ has positive diagonal elements [15]. Furthermore, one can readily verify that

$$\mathcal{M}_5 = \mathcal{L}_\mathcal{M} \mathcal{L}_\mathcal{M}^t, \tag{79}$$

where

$$\mathcal{L}_\mathcal{M} = \begin{bmatrix} \mathcal{W}\mathcal{L}_\mathcal{S} & \vec{0} \\ -\mathcal{A}^t\mathcal{L}_\mathcal{S} & 0 \end{bmatrix}. \tag{80}$$

Since $\mathcal{W}$ has positive diagonal elements, the product $\mathcal{W}\mathcal{L}_\mathcal{S}$ is lower-triangular with positive diagonal elements. Therefore, $\mathcal{L}_\mathcal{M}$ is lower-triangular with 4 positive diagonal elements and 1 zero diagonal element. This demonstrates that $\mathcal{M}_5$ has a Cholesky decomposition.

We now determine the null space of $\mathcal{M}_5$ by finding all solutions $(\vec{b}, \nu)$ to the equation

$$\mathcal{M}_5 \begin{bmatrix} \vec{b} \\ \nu \end{bmatrix} = \begin{bmatrix} \vec{0} \\ 0 \end{bmatrix}. \tag{81}$$

These solutions form the null space of $\mathcal{M}_5$. Straightforward algebraic manipulation of Eq. (81) reveals that

$$\text{null}(\mathcal{M}_5) = \text{span}\left\{\begin{bmatrix}\mathcal{W}^{-1}\mathcal{A}\\ 1\end{bmatrix}\right\}, \tag{82}$$

$$= \text{span}\left\{\begin{bmatrix}1\\ \vdots\\ 1\end{bmatrix}\right\} \in \mathcal{R}^{5\times 1}. \tag{83}$$

Equivalently, any vector will satisfy Eq. (81) if it has the form

$$\vec{\phi} = \alpha(1, 1, 1, 1, 1), \tag{84}$$

where α is any real number.

To determine that the matrix resulting from a multi-cell mesh with reflective boundary conditions is SPS, we first define a single-cell matrix for each cell in a multi-cell mesh, and denote each one by $\mathcal{M}_{5,c}$ where c is the cell index. We next assume that there are a total of N intensity unknowns on the multi-cell mesh, and re-express each matrix $\mathcal{M}_{5,c}$ as a full $N \times N$ matrix. We denote this matrix by $\mathcal{M}_{N,c}$,

$$\mathcal{M}_{5,c} \in \mathcal{R}^{5\times 5} \rightarrow \mathcal{M}_{N,c} \in \mathcal{R}^{N\times N}. \tag{85}$$

To establish the null-space of $\mathcal{M}_{N,c}$, we first define $\mathbf{B}_c$ as the set of indices for the intensities contained in cell c:

$$\mathbf{B}_c \equiv \{\text{all } i \text{ such that } (\mathcal{M}_{N,c})_{i,i} \neq 0\}. \tag{86}$$

Recalling the null space of $\mathcal{M}_{5,c}$, it follows that

$$\text{null}(\mathcal{M}_{N,c}) = \text{span}\{(\phi_1, \phi_2, \ldots, \phi_N)\}, \tag{87}$$

where $\phi_i = 1$ if $i \in \mathbf{B}_c$, and ϕ_i is otherwise arbitrary. This null space has a dimension of $N - 4$.

We now demonstrate the effect of summing the single-cell matrices from two adjacent cells. Consider two adjacent cells with indexes $c1$ and $c2$. Without loss of generality, we assume that these cells are oriented such that the right face of cell $c1$ is also the left face of cell $c2$. Let us next consider the intensity at the interface between the two cells, which we denote by $\phi_{c1|c2}$. It is important to recognize that only $\mathcal{M}_{N,c1}$ and $\mathcal{M}_{N,c2}$ have an equation for this intensity. The equation for $\phi_{c1|c2}$ given by $\mathcal{M}_{N,c1}$ is

$$-A^R_{c1} f^R_{c1} = 0, \tag{88}$$

while the equation for $\phi_{c1|c2}$ given by $\mathcal{M}_{N,c2}$ is

$$-A^L_{c2} f^L_{c2} = 0. \tag{89}$$

Note that when these equations are added together, the correct continuity-of-flux equation for $\phi_{c1|c2}$ (see Eq. (20)) is obtained:

$$-A^R_{c1} f^R_{c1} - A^L_{c2} f^L_{c2} = 0. \tag{90}$$

Therefore, the sum over all c of $\mathcal{M}_{N,c}$ yields the diffusion matrix for our support-operators scheme with Neumann conditions on the outer boundary faces. We denote this matrix as

$$\mathcal{M}' = \sum_c \mathcal{M}_{N,c}. \tag{91}$$

This matrix is SPS, since the sum of matrices with Cholesky decompositions is guaranteed to be SPS. The null space of a sum of matrices with Cholesky decompositions is the intersection of the cell matrix null spaces,

$$\text{null}(\mathcal{M}') = \bigcap_c \text{null}(\mathcal{M}_{N,c}). \tag{92}$$

Since the union of all of the $\mathbf{B}_c$ is the set from 1 to N,

$$\bigcup_c \mathbf{B}_c = \{1, 2, \ldots, N\}, \tag{93}$$

the null space of $\mathcal{M}'$ contains all vectors with the same value in all of its columns:

$$\text{null}(\mathcal{M}') = \text{span}\left\{ \begin{bmatrix} 1 \\ \vdots \\ 1 \end{bmatrix} \right\} \in \mathcal{R}^{N\times 1}. \tag{94}$$

Now we assume that there is at least one cell, v, that has a face with an extrapolated boundary condition. At least one such face must exist to ensure that a unique solution to the steady-state version of Eq. (1) exists. Without loss of generality, we assume that this face is the rightmost face. The extrapolated boundary conditions for this face can be expressed in the form

$$A_v^R\left(\lambda_v^R \phi_v^R - f_v^R\right) = A_v^R \lambda_v^R \phi_{v,e}^R. \tag{95}$$

Although it might not be obvious, this form is equivalent to that expressed in Eq. (24). For instance, the Marshak boundary condition is obtained if $\lambda_v^R = 0.5$.

This face equation will contribute an additional term to the sum in Eq. (91). This yields the final support-operators diffusion matrix that we seek: the matrix for a multi-cell mesh with an extrapolated boundary condition at one face, and Neumann boundary conditions at all of the other faces. We denote this matrix by $\mathcal{M}$,

$$\mathcal{M} = \sum_c \mathcal{M}_{N,c} + \mathcal{M}'_v, \tag{96}$$

where the matrix $\mathcal{M}'_v$ contains only one non-zero element, $A_v^R \lambda_v^R$, which is located on the diagonal corresponding to the intensity on the extrapolated boundary face:

$$\mathcal{M}'_v = \begin{bmatrix} 0 & 0 & 0 \\ 0 & A_v^R \lambda_v^R & 0 \\ 0 & 0 & 0 \end{bmatrix} \in \mathcal{R}^{N\times N}. \tag{97}$$

The matrix, $\mathcal{M}'_v$, with only one non-zero element that is positive and located on the diagonal, obviously has a Cholesky decomposition. Its null space contains all vectors with

a zero in the location corresponding to the intensity on the extrapolated boundary face. It is obvious that this null space is disjoint from the intersection of the null spaces of the matrices forming the sum in Eq. (91), and therefore

$$\text{null}(\mathcal{M}) = \bigcap_c \text{null}(\mathcal{M}_{N,c}) \bigcap \text{null}(\mathcal{M}'_v), \tag{98}$$

$$= \emptyset, \tag{99}$$

the empty set. Using the theorem proved at the beginning of this Appendix, we have demonstrated that $\mathcal{M}$ is SPD.

APPENDIX C

In this appendix we demonstrate that our new solution method preserves the spherical symmetry of a solution on a spherically symmetric mesh. A spherically symmetric r-z mesh is illustrated in Fig. 20. The mesh coordinates are labeled with the i axis in the $\vec{\theta}$ direction and the j axis in the $\vec{R}$ direction, where

$$R = \sqrt{r^2 + z^2}. \tag{100}$$

In order to demonstrate that this scheme perserves a spherically symmetric solution we will show that the new scheme admits a solution with cell-center intensities independent of the i coordinate, i.e.,

$$\phi^C_{i,j} = \phi^C_j, \tag{101}$$

and that these symmetric intensities lead to fluxes, $f_{i,j}$, independent of i, having only radial

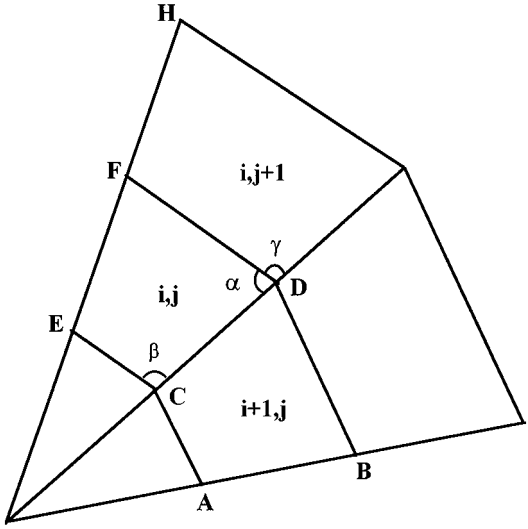

FIG. 20. The spherically symmetric mesh.

components, i.e.,

$$\begin{aligned} f^B_{i,j} &= f^B_j, \\ f^T_{i,j} &= f^T_j, \\ f^R_{i,j} &= 0, \\ f^L_{i,j} &= 0. \end{aligned} \tag{102}$$

To establish the above relations we must first show that the factor used to scale the volumetric weights in Eq. (37) is independent of i,

$$W_{i,j} = \frac{V_{i,j}}{\tilde{V}^{TR}_{i,j} + \tilde{V}^{RB}_{i,j} + \tilde{V}^{BL}_{i,j} + \tilde{V}^{LT}_{i,j}}, \tag{103}$$

$$= W_j. \tag{104}$$

The unnormalized volumetric weights for the corners are related to the parallelepiped volumes, $\mathcal{V}$, by

$$\tilde{V}^{TR}_{i,j} = 2\pi r_{i+\frac{1}{2},j+\frac{1}{2}} \mathcal{V}^{TR}_{i,j}, \tag{105}$$

$$\tilde{V}^{RB}_{i,j} = 2\pi r_{i+\frac{1}{2},j-\frac{1}{2}} \mathcal{V}^{RB}_{i,j}, \tag{106}$$

$$\tilde{V}^{BL}_{i,j} = 2\pi r_{i-\frac{1}{2},j-\frac{1}{2}} \mathcal{V}^{BL}_{i,j}, \tag{107}$$

$$\tilde{V}^{LT}_{i,j} = 2\pi r_{i-\frac{1}{2},j+\frac{1}{2}} \mathcal{V}^{LT}_{i,j}. \tag{108}$$

Due to the regularity of this mesh the parallelpiped volumes are simply related,

$$\mathcal{V}^{TR}_{i,j} = \mathcal{V}^{LT}_{i,j} = \mathcal{V}_{j+\frac{1}{2}}, \tag{109}$$

$$\mathcal{V}^{RB}_{i,j} = \mathcal{V}^{BL}_{i,j} = \mathcal{V}_{j-\frac{1}{2}}, \tag{110}$$

where

$$\mathcal{V}_{j-\frac{1}{2}} = \frac{R_{j-\frac{1}{2}}}{R_{j+\frac{1}{2}}} \mathcal{V}_{j+\frac{1}{2}}, \tag{111}$$

and the expression for the volumetric weight scaling factor, Eq. (103), is

$$W_j = \frac{1}{6} \frac{R^2_{j-\frac{1}{2}} + R_{j-\frac{1}{2}} R_{j+\frac{1}{2}} + R^2_{j+\frac{1}{2}}}{R^2_{j-\frac{1}{2}} + R^2_{j+\frac{1}{2}}}, \tag{112}$$

where Eq. (38) was substituted for $V_{i,j}$.

There are two sets of equations that we will examine. The first set is used to find an expression for $f^T_{i,j}$ from cell $i,\ j$ and its top neighbor, cell $i,\ j+1$. This expression will be found to be independent of i for a spherically symmetric problem. The second set is used to find an expression for $f^R_{i,j}$ from cell $i,\ j$ and its right neighbor, cell $(i+1,\ j)$. This expression will be found to be zero for a spherically symmetric problem. Due to current continuity we will not need to examine $f^B_{i,j}$, nor $f^L_{i,j}$. These expressions will be derived referring to Fig. 20.

To derive an expression for $f^T_{i,j}$, we use the ϕ^T equation for cell i, j and the ϕ^B equation for cell i, $j+1$:

$$\frac{V^{LT}_{i,j}}{\sin^2\alpha}\left(f^T_{i,j}+\cos\alpha f^L_{i,j}\right)+\frac{V^{TR}_{i,j}}{\sin^2\alpha}\left(f^T_{i,j}+\cos\alpha f^R_{i,j}\right)=-DA^T_{i,j}\left(\phi^T_{i,j}-\phi^C_{i,j}\right) \quad (113)$$

$$\frac{V^{BL}_{i,j+1}}{\sin^2\gamma}\left(f^B_{i,j+1}+\cos\gamma f^L_{i,j+1}\right)+\frac{V^{RB}_{i,j+1}}{\sin^2\gamma}\left(f^B_{i,j+1}+\cos\gamma f^R_{i,j+1}\right)$$
$$=-DA^B_{i,j+1}\left(\phi^B_{i,j+1}-\phi^C_{i,j+1}\right). \quad (114)$$

The $\sin^2\alpha$ and $\sin^2\gamma$ terms arise from the form of the $\mathcal{S}^{-1}$-matrix (see Eq. (34)).

We now rely on the continuity between neighbor cells, i.e.,

$$\phi^B_{i,j+1}=\phi^T_{i,j}, \quad (115)$$
$$f^B_{i,j+1}=-f^T_{i,j}, \quad (116)$$

and geometric relations between the two cells,

$$\sin\gamma=\sin\alpha, \qquad \text{independent of } i, \quad (117)$$

to eliminate the face-center unknown, $\phi^T_{i,j}$, from the equations. In doing so we assume that the intensities and volume scaling factors depend only on j, and that $f^L=f^R=0$,

$$\frac{W_j+W_{j+1}}{\sin^2\alpha}\mathcal{V}_{j+\frac{1}{2}}f^T_{i,j}=-\frac{1}{2}D\left\|\Delta\vec{r}_{j+\frac{1}{2}}\right\|\left(\phi^C_{j+1}-\phi^C_j\right), \quad (118)$$

with

$$\left\|\Delta\vec{r}_{j+\frac{1}{2}}\right\|=\left\|\vec{r}_{i+\frac{1}{2},j+\frac{1}{2}}-\vec{r}_{i-\frac{1}{2},j+\frac{1}{2}}\right\|, \qquad \text{independent of } i. \quad (119)$$

We have used Eqs. (21), (30), (104), (105)–(108), and (109) to arrive at Eq. (118). It is clear that $f^T_{i,j}$ depends only on j:

$$f^T_{i,j}=f^T_j. \quad (120)$$

Now that we have shown that the first set of equations, with the assumption of radial fluxes, yields spherically symmetric fluxes, we will demonstrate that spherically symmetric fluxes yield radial fluxes for the second set of equations.

To derive an expression for $f^R_{i,j}$ we use the ϕ^R equation for cell i, j and the ϕ^L equation for cell $i+1$, j, respectively,

$$\frac{V^{TR}_{i,j}}{\sin^2\alpha}\left(f^R_{i,j}+\cos\alpha f^T_{i,j}\right)+\frac{V^{RB}_{i,j}}{\sin^2\beta}\left(f^R_{i,j}+\cos\beta f^B_{i,j}\right)=-DA^R_{i,j}\left(\phi^R_{i,j}-\phi^C_{i,j}\right), \quad (121)$$

$$\frac{V^{LT}_{i+1,j}}{\sin^2\alpha}\left(f^L_{i+1,j}+\cos\alpha f^T_{i+1,j}\right)+\frac{V^{BL}_{i+1,j}}{\sin^2\beta}\left(f^L_{i+1,j}+\cos\beta f^B_{i+1,j}\right)$$
$$=-DA^L_{i+1,j}\left(\phi^L_{i+1,j}-\phi^C_{i+1,j}\right). \quad (122)$$

We now rely on the continuity between neighbor cells, i.e.,

$$\phi^L_{i+1,j} = \phi^R_{i,j}, \tag{123}$$

$$f^L_{i+1,j} = -f^R_{i,j}, \tag{124}$$

and geometric relations between the two cells,

$$\sin\beta = \sin\alpha, \qquad \text{independent of } i, \tag{125}$$

$$V^{LT}_{i+1,j} = V^{TR}_{i,j}, \tag{126}$$

$$V^{BL}_{i+1,j} = V^{RB}_{i,j}, \tag{127}$$

to eliminate $f^L_{i+1,j}$ and the face-center unknowns, $\phi^R_{i,j}$ and $\phi^L_{i+1,j}$, from Eqs. (121) and (122). In doing so we assume that the intensities, $\phi^C_{i,j}$, volume scaling factors, $W_{i,j}$, and radial fluxes, $f^T_{i,j}$ and $f^B_{i,j}$, depend only on j (independent of i). Equations (121) and (122) become

$$\frac{2}{\sin^2\alpha}\left[V^{TR}_{i,j} + V^{RB}_{i,j}\right] f^R_{i,j} = -DA^R_{i,j}\left(\phi^C_{i+1,j} - \phi^C_{i,j}\right), \tag{128}$$

$$= -DA^R_{i,j}\left(\phi^C_j - \phi^C_j\right), \tag{129}$$

$$= 0. \tag{130}$$

Since the factor in front of $f^R_{i,j}$ is non-zero, we must conclude that

$$f^R_{i,j} = 0, \tag{131}$$

which implies that a spherically symmetric initial solution results in a radial flux.

We have succeeded in demonstrating that the new method, on a spherically symmetric r-z mesh, preserves a spherical solution that consists of fluxes with only non-zero radial components.

ACKNOWLEDGMENT

This work was performed under the auspices of the U.S. Department of Energy.

REFERENCES

1. G. C. Pomraning, *Equations of Radiation Hydrodynamics*, in International Series of Monographs in Natural Philosophy, edited by D. ter Haar (Pergamon, New York, 1973), Vol. 54.
2. O. C. Zienkiewicz, *The Finite Element Method* (McGraw–Hill, London, 1977), 3rd ed.
3. A. I. Shestakov, J. A. Harte, and D. S. Kershaw, Solution of the diffusion equation by finite elements in Lagrangian hydrodynamics codes, *J. Comput. Phys.* **76**, 385 (1988).
4. D. S. Kershaw, Differencing of the diffusion equation in Lagrangian hydrodynamic codes, *J. Comput. Phys.* **39**, 375 (1981).
5. G. J. Pert, Physical constraints in numerical calculations of diffusion, *J. Comput. Phys.* **42**, 20 (1981).
6. J. E. Morel, J. E. Dendy, Jr., M. Hall, and S. White, A cell-centered Lagrangian-mesh diffusion differencing scheme, *J. Comput. Phys.* **103**, 286 (1992).

7. P. Van Beek, R. R. P. Van Nooyen, and P. Wesseling, Accurate discretization of gradients on non-uniform staggered grids, *J. Comput. Phys.* **117**, 364 (1995).
8. I. Aavatsmark, T. Barkve, Ø. Bøe, and T. Mannseth, Discretization on non-orthogonal, quadrilateral grids for inhomogeneous, anisotropic media, *J. Comput. Phys.* **127**, 2 (1996).
9. M. J. Shashkov and S. Steinberg, Solving diffusion equations with rough coefficients in rough grids, *J. Comput. Phys.* **129**, 383 (1996).
10. D. N. Arnold and F. Brezzi, Mixed and nonconforming finite element methods: Implementation, post processing, and error estimates, *Math. Model. Numer. Anal.* **19**, 7 (1985).
11. T. Arbogast, C. N. Dawson, P. T. Keenan, M. F. Wheeler, and I. Yotov, Enhanced cell-centered finite differences for elliptic equations on general geometry, *SIAM J. Sci. Comput.* **18**, 1 (1997).
12. Z. Cai, J. E. Jones, S. F. McCormick, and T. F. Russell, *Comput. Geosci.* **1**(3) (1997).
13. G. H. Golub and C. F. Van Loan, *Matrix Computations* (Johns Hopkins Press, Baltimore, 1983).
14. J. E. Dendy, Jr., Black box multigrid, *J. Comput. Phys.* **48**, 366 (1982).
15. J. Stoer and R. Bulirsch, *Introduction to Numerical Analysis* (Springer-Verlag, New York, 1980).